

An ultrasensitive SiO₂-encapsulated alloyed CdZnSeS quantum dot-molecular beacon nanobiosensor for norovirus

メタデータ	言語: eng 出版者: 公開日: 2018-06-12 キーワード (Ja): キーワード (En): 作成者: Adegoke, Oluwasesan, Seo, Min-Woong, Kato, Tatsuya, Kawahito, Shoji, Park, Enoch Y. メールアドレス: 所属:
URL	http://hdl.handle.net/10297/00025260

An ultrasensitive SiO₂-encapsulated alloyed CdZnSeS quantum dot-molecular beacon nanobiosensor for norovirus

Oluwasesan Adegoke,^a Min-Woong Seo,^b Tatsuya Kato,^{a,c} Shoji Kawahito,^b Enoch Y. Park^{a,c*}

^a *Laboratory of Biotechnology, Research Institute of Green Science and Technology, Shizuoka University, 836 Ohya, Suruga-ku, Shizuoka 422-8529, Japan*

^b *Imaging Devices Laboratory, Research Institute of Electronics, Shizuoka University, Johoku 3-5-1, Naka-ku, Hamamatsu 432-8011, Japan*

^c *Laboratory of Biotechnology, Department of Bioscience, Graduate School of Science and Technology, Shizuoka University, 836 Ohya, Suruga-ku, Shizuoka 422-8529, Japan*

E-mail:

adegoke.sesan@mailbox.co.za (OA)

mwseo@idl.rie.shizuoka.ac.jp (MS)

kawahito@idl.rie.shizuoka.ac.jp (SK)

kato.tatsuya@shizuoka.ac.jp (TK)

park.enoch@shizuoka.ac.jp (EYP)

* Corresponding author: Research Institute of Green Science and Technology, Shizuoka University, 836 Ohya, Suruga-ku, Shizuoka 422-8529, Japan.

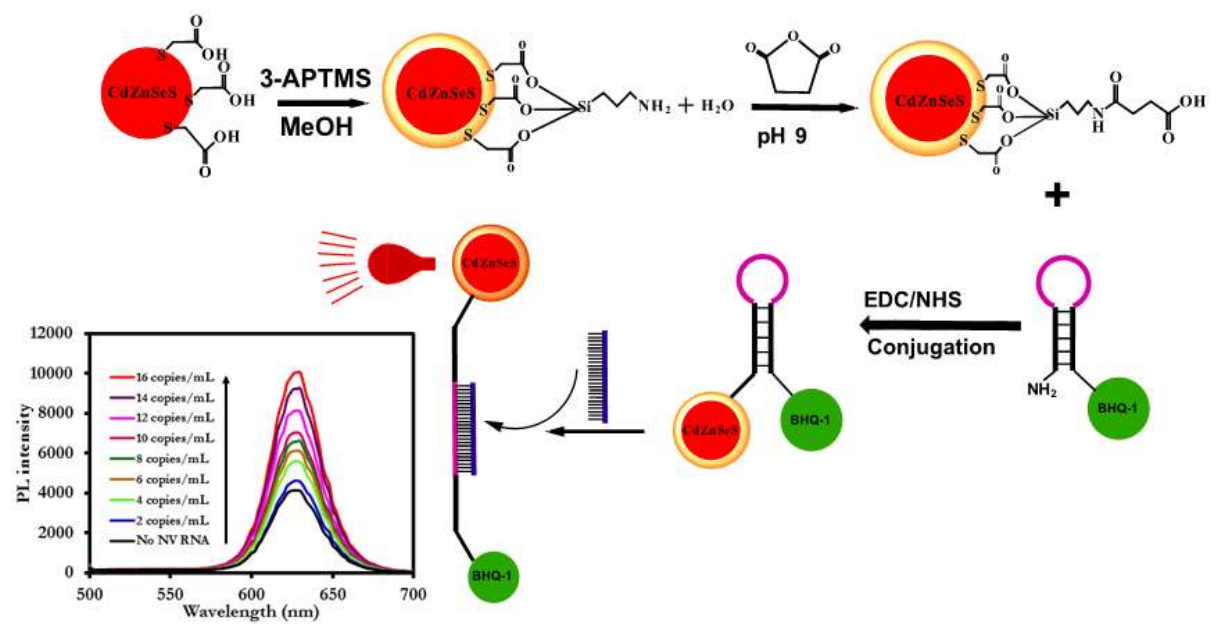
E-mail: park.enoch@shizuoka.ac.jp (EYP). Phone & Fax: +81-54-238-4887

ABSTRACT

Ultrasensitive, rapid and selective diagnostic probes are urgently needed to overcome the limitations of traditional probes for norovirus (NV). Here, we report the detection of NV genogroup II via nucleic acid hybridization technology using a quantum dot (QD)-conjugated molecular beacon (MB) probe. To boost the sensitivity of the MB assay system, an ultrasensitive QD fluorophore with unique optical properties was synthesized, characterized and exploited as a fluorescence signal generator. Alloyed thioglycolic (TGA)-capped CdZnSeS QDs with a high photoluminescence (PL) quantum yield (QY) value of 92% were synthesized, and a modified silanization method was employed to encapsulate the thiol-capped QDs in a silica layer. The resulting highly luminescent alloyed SiO₂-coated CdZnSeS QDs had a remarkable PL QY value of 98%. Transmission electron microscopy and dynamic light scattering confirmed the monodispersity of the alloyed nanocrystals, and zeta potential analysis confirmed their colloidal stability. Powder X-ray diffraction and PL lifetime measurements confirmed the surface modification of the QDs. The alloyed TGA-capped and SiO₂-coated CdZnSeS QD-conjugated MB bioprobes detected extremely low concentrations of NV RNA. Ultrasensitive detection of low concentrations of NV RNA with a limit of detection (LOD) of 8.2 copies/mL in human serum and a LOD of 9.3 copies/mL in buffer was achieved using the SiO₂-coated CdZnSeS QD-MB probes, an increase in sensitivity of 3-fold compared with the detection limit for NV RNA using TGA-capped CdZnSeS QD-MBs. The additional merits of our detection system are rapidity, specificity and improved sensitivity over conventional molecular test probes.

Keywords: molecular beacon, quantum dots, alloy, norovirus virus, RNA, bioprobe

Graphical abstract



1. Introduction

Noroviruses (NVs) are the leading etiological viral agent of acute gastroenteritis and are the predominant causative agents of outbreaks of foodborne disease (**Ando et al., 1995; Rooney et al., 2014**). Conventional diagnostic techniques for NV have certain limitations. For example, enzyme immunoassays and rapid immunochromatographic assays exhibit contrasting sensitivities, and the former is not useful for point-of-care or nucleic acid amplification testing (**Robilotti et al., 2015**). Molecular diagnostic tests employing RT-PCR are limited by post-amplification specimen handling, assay complexity and the requirement for accurate performance tests (**Robilotti et al., 2015**). There is therefore an urgent demand for diagnostic probes that can offer accurate, rapid detection, high sensitivity and high specificity for NV.

Molecular beacon (MB) probes have been employed extensively in chemical and biological research, including in genotyping (**Kostrikis et al., 1998**), single nucleotide detection by PCR (**Barreiro et al., 2009**), mutation detection (**Hodgson et al., 2002**), cancer-cell detection (**Medley et al., 2005**), assays for nucleic acid cleavage (**Li et al., 2000**) and monitoring viral infection (**Santangelo et al., 2006**). For biosensor applications, a key consideration in the design of a MB probe is the choice of the fluorophore reporter. To generate a novel fluorescent signal for the detection of the target analyte, the fluorophore reporter must exhibit unique optical properties. Semiconductor quantum dot (QD) nanocrystals are an excellent choice as a fluorophore reporter compared to organic dyes due to their size-tunable absorption and fluorescence spectra, narrow emission and broad absorption spectra, color tunability, excellent photostability and low resistance to photodegradation (**Anderson and Chan, 2008; Bruchez et al., 2013; Chan and Nie, 1998**). The chemistry of QDs can be tailored by producing alloyed nanocrystals. Alloyed QDs enable improved flexibility in output efficiency compared to conventional QD systems (**Wang et al., 2009; Ma et al., 2009; Caruge**

et al., 2008). Different alloyed QD cores for ternary and quaternary structures have been reported (**Ünlü et al., 2013; Swafford et al., 2006; Adegoke et al., 2015**).

We recently reported a new method for viral nucleic acid fluorescence detection using an alloyed QD-MB biosensor probe (**Adegoke et al., 2016**). We demonstrated the ultrasensitive nature of the detection system based on the choice of fluorophore reporter. Ultrasensitive alloyed core/shell QDs with high photoluminescence (PL) quantum yield (QY) were used as the fluorophore reporter to generate an unparalleled fluorescent signal for the detection of extraordinarily low concentrations of influenza virus RNA (**Adegoke et al., 2016**). We have continued to develop alloyed QD systems with unique optical properties for use as ultrasensitive fluorescence signal generators in viral nucleic acid detection.

In this work, water-soluble alloyed quaternary CdZnSeS QD nanocrystals were synthesized. First, an organometallic hot-injection method was used to fabricate the hydrophobic CdZnSeS QDs, and a ligand-exchange reaction using thioglycolic acid (TGA) as the thiol ligand was used to obtain water-soluble nanocrystals. We further employed a modified silanization method to improve the optical properties of the alloyed QDs. The modified SiO₂-coated alloyed CdZnSeS QDs exhibited a remarkable PL QY value of 98%. We then demonstrated the bioanalytical potential of the SiO₂-coated CdZnSeS QD-conjugated MB probe as an ultrasensitive fluorescence biosensor for the detection of extremely low concentrations of NV genogroup II RNA. The ultrasensitive feature of our probe system is the unprecedented fluorescent signal generated by the SiO₂-coated CdZnSeS fluorophore reporter. We exploited the versatility of our probe system by demonstrating its efficacy for the detection of the target NV RNA in complex biological matrix. For comparison, we explored the potential of alloyed TGA-CdZnSeS-MB to detect extremely low concentrations of the target NV RNA. The SiO₂-coated alloyed CdZnSeS-MB nanodiagnostic bioprobe developed in this work for NV RNA is the first of its kind and is rapid, specific, versatile and ultrasensitive.

2. Materials and methods

2.1. Materials

Cadmium oxide (CdO), octadecene (ODE), zinc oxide (ZnO), trioctylphosphine oxide (TOPO), trioctylphosphine (TOP), selenium (Se), hexadecylamine (HDA), sulfur, (3-aminopropyl)trimethoxysilane (3-APTMS), chlorotrimethylsilane, tetramethylammonium hydroxide (TMAH) pentahydrate, succinic anhydride, rhodamine 6G, N-(3-dimethylaminopropyl)-N'-ethylcarbodiimide hydrochloride (EDC), N-hydroxysuccinimide (NHS) and TGA were purchased from Sigma Aldrich Co. LLC (Saint Louis, MO, USA). Oleic acid was purchased from Nacalai Tesque Inc. (Kyoto, Japan). Potassium hydroxide (KOH), methanol, acetone and chloroform were purchased from Wako Pure Chemical Ind. Ltd. (Osaka, Japan). An ultra-pure Milli-Q Water System was used as the water source. Target complimentary NV RNA of genogroup II (G11), non-complimentary dengue 1 virus RNA and influenza virus A/California/07/2009 (H1N1) were purchased from Vircell Microbiologists (Granada, Spain). The MB with a DNA oligonucleotide was synthesized and purified by HPLC by FASMAC (Kanagawa, Japan). The MB consisted of a 30-bp single-stranded DNA labeled at the 5' terminus with an amino group (NH₂) and at the 3' terminus with the fluorescence quencher BHQ-1 (black hole quencher 1). The MB probe contained 20 bp complementary to NV genogroup II RNA. The resulting oligonucleotide sequence of the MB was as follows:

5'-/NH₂-/GCGACGAATTAGCTTGTATGATGTCGTCGC-BHQ1/-3'.

The underlined bases correspond to the stem domain.

2.2. Equipment

UV/vis absorption and fluorescence emission measurements were performed using a filter-based multimode microplate reader (Infinite® F500, TECAN, Ltd, Männedorf, Switzerland). Transmission electron microscopy (TEM) images were captured using a TEM JEM-2100F,

(JEOL, Ltd., Tokyo, Japan) operated at 100 kV. Powder X-ray diffraction (PXRD) measurements were obtained using a RINT ULTIMA XRD (Rigaku Co., Tokyo, Japan) with a Ni filter and a Cu-K α source. Data were collected from $2\theta = 5\text{--}60^\circ$ at a scan rate of $0.01^\circ/\text{step}$ and $10\text{ s}/\text{point}$. Fourier transform infrared spectroscopy (FT-IR) analyses were conducted using an FT-IR instrument (ATR 8700, Shimadzu Co., Tokyo, Japan). Zeta potential and dynamic light scattering (DLS) analyses were performed using a Zetasizer Nano series. Fluorescence lifetime measurements were obtained by fluorescence lifetime imaging microscopy (FLIM) with a time-resolved CMOS image sensor (Seo et al., 2015). The excitation source was a 472-nm laser diode with a pulse width of 120 ps and a peak power of 48 mW. The cycle period of the trigger signal was 192 ns, the width of the time window was 26 ns, the delay step for scanning was 500 ps, and the sensor's intrinsic response to the 472-nm laser was 220 ps.

2.3. Silica encapsulation of alloyed CdZnSeS QDs

First, alloyed TGA-capped CdZnSeS QDs were synthesized based on our recent report (Adegoke et al, 2016). The alloyed TGA-capped CdZnSeS QDs were silanized according to a reported procedure (Wu et al., 2011) with modifications. The amino-silanized QDs were prepared by mixing 10 mL of 3-APTMS with 5 mL of methanol and added to 10 mL of an aqueous alloyed QD solution at room temperature with vigorous stirring. The solution was allowed to stir for ~ 10 min and then heated at $\sim 60^\circ\text{C}$ for ~ 30 min. To quench the silanization reaction, 80 mL of methanol was added to the QD solution, swiftly followed by the addition of 3 mL of chlorotrimethylsilane basified with 3.75 g of solid TMAH pentahydrate. The solution was stirred for ~ 2 hr and was then heated at $\sim 60^\circ\text{C}$ for ~ 30 min. The amino-silanized alloyed QDs were precipitated from solution by acetone and further washed with chloroform.

The carboxyl-silanized alloyed QDs were prepared by suspending the wet precipitate of the amino-silanized QDs in phosphate buffer, pH 9, and 1.0 g of succinic anhydride was added and dissolved ultrasonically. The solution was stirred overnight at ambient temperature. The carboxyl-silanized alloyed QDs were precipitated from solution by acetone and further washed with chloroform.

2.4. Preparation of the SiO₂-coated CdZnSeS-MB bioprobe

An aqueous solution (2.5 mL) of alloyed SiO₂-CdZnSeS QDs (0.6 mg/mL) in phosphate buffer (pH ~7.4) was stirred in a capped vial with 1.0 mL of aqueous 0.1 M EDC. The reaction was allowed to proceed for ~35 min to activate the carboxylate groups on the QD surface. Then, 1.0 mL of ~10 nM MB (prepared in Tris-EDTA buffer, pH ~8.0) and 1.0 mL of 0.1 M NHS solution were added to the EDC-activated alloyed QDs and reacted overnight at ambient temperature. The alloyed QD-MB conjugate was concentrated and purified by centrifugation in a 30,000 Microcon molecular weight cut-off Nanosep® centrifugal filter (Pall Co., Port Washington, NY, USA). The QD-MB conjugate solution was stored at 4 °C prior to use.

2.5. Fluorescence detection assay

In a 96-well plate, 1 µL of purified alloyed QD-MB solution was mixed with 50 µL of buffer or human serum and 5 µL of the target NV RNA. Each concentration of NV was detected under the same experimental conditions. For each concentration of NV RNA detected, an hybridization time of 3 min was employed to allow the DNA oligonucleotide sequence to hybridize with the target RNA sequence. Triplicate measurements were performed for each concentration of NV. The excitation wavelength was fixed at 470 nm, and the PL emission range was measured between 480 and 800 nm.

2.6. Fluorescence detection principle

Scheme 1 illustrates the detection principle of the alloyed QD-MB bioprobe for NV RNA. The terminal carboxyl functional group of the alloyed QDs was conjugated to the terminal amino moiety at the 5' end of the MB to form a covalent amide bond linkage. In the absence of the target NV RNA, the alloyed QDs and the quencher molecule are in close proximity. However, in the presence of the target RNA, the hybridization of the DNA oligonucleotide loop sequence of the MB with the RNA sequence of the target NV results in a DNA/RNA heteroduplex that stretches the distance between the alloyed QD reporter and the quencher molecule. The hybridization effect allows the alloyed QD reporter to generate a fluorescent signal that is proportional to the concentration of NV RNA.

3. Results and discussion

3.1. Structural properties

3.1.1. Morphology of alloyed CdZnSeS QDs

Scheme 1 provides a description of the silica-encapsulation procedure employed to modify the surface of the alloyed CdZnSeS QDs. The major steps of this process were as follows: (i) ligand phase transfer, (ii) silanization with the 3-APTMS precursor in an aqueous medium and (iii) conversion of the primary amine group to a carboxyl functional group with succinic anhydride in an alkaline medium. Figure 1A-C shows the TEM images (same sample, different magnifications) of the alloyed TGA-capped CdZnSeS QDs, and Fig. 1D-F shows the corresponding images of SiO₂-coated CdZnSeS QDs. A high degree of monodispersity and homogeneity in the particle distribution of TGA-capped and SiO₂-coated CdZnSeS QDs was achieved, as indicated in each image magnification. The morphological assembly of the nanocrystals revealed the formation of a quasi-spherical pattern of particles that remained consistent throughout the entire TEM monograph. Observing the embedding of the QDs in the

silica layer is difficult from the TEM images of the SiO₂-coated CdZnSeS QDs, most likely because of the structural nature and surface properties of the alloyed QDs. Generally, we can infer that upon silanization of the alloyed QDs, the particle size distribution and the morphological assembly of the QDs were not distorted. We attribute this stability to the effective silanization procedure, which modified the QD surface while retaining its morphological pattern. The average particle size distribution for TGA-CdZnSeS QDs was estimated as 5.9 nm, which increased to 6.7 nm upon formation of the SiO₂-coated CdZnSeS QDs. Tentatively, we estimate that a silica shell layer with a thickness of ~0.4 nm was coated **around** the alloyed QDs.

3.1.2. Hydrodynamic particle size and zeta potential

An important tool for the size characterization of nanoparticles in solution is DLS. This technique is also essential in probing the monodispersity or polydispersity of nanoparticles in solution. If both TGA-capped and SiO₂-coated CdZnSeS QDs have a high polydispersity index and are aggregated, the measured DLS hydrodynamic size will be extremely large compared with the TEM size. Suspensions of aggregated nanoparticles generally have a hydrodynamic size in the range of 100–300 nm. By contrast, if the alloyed nanocrystals do not aggregate, the hydrodynamic size will be slightly larger or similar to the value determined by TEM. Figures 2A and B show the DLS curves for TGA-capped and SiO₂-coated CdZnSeS QDs. The monodispersity of the nanocrystals was confirmed by the DLS hydrodynamic size. The hydrodynamic size obtained for alloyed TGA-CdZnSeS was 5.1 nm, similar to the TEM value of 5.9 nm. The measured hydrodynamic size of the alloyed SiO₂-coated CdZnSeS QDs was 44.9 nm, larger than the TEM value but still within the range of nanocrystal monodispersity. It is important to note that the DLS data of TGA QDs and silica-coated QDs are not expected to have the same degree of dispersity in solution due to differences in the surface capping. TGA-

QDs has a thiol ligand on its surface and silica-coated QDs has a silica layer on its surface. The differences in surface-capping will induce different steric repulsion in solution which will influence the hydrodynamic size results

The zeta potentials of the alloyed nanocrystals were measured to probe their colloidal stability in solution. Zeta potential values are usually in the range of -100 mV to +100 mV. The long-term stability of alloyed nanocrystals can be predicted from the magnitude of the zeta potential. Nanoparticles with zeta potentials in the range of -10 and +10 mV are considered neutral, but if this value is greater than +30 mV or lower than -30 mV, the nanoparticles are considered strongly cationic or strongly anionic (**Cloqston et al., 2011**). Strongly cationic or strongly anionic nanoparticles are considered to exhibit a high degree of colloidal stability. Figures 2C and D present the zeta potential curves of TGA-capped and SiO₂-coated CdZnSeS QDs exhibiting a single symmetric Gaussian peak. The zeta potential value was -63.4 mV for alloyed TGA-CdZnSeS QDs and -58.0 mV for SiO₂-coated CdZnSeS QDs. These values indicate that both TGA-capped and SiO₂-coated CdZnSeS QDs exhibit a high degree of colloidal stability in solution.

3.1.3. PXRD

PXRD analysis was performed to confirm the crystallinity of the alloyed nanocrystals. Figure 3 shows the XRD patterns of TGA-capped and SiO₂-coated CdZnSeS QDs. The diffraction patterns of both alloyed nanocrystals exhibit a notable zinc-blend crystal structure with peaks indexed to the {111}, {220} and {311} planes. The diffraction pattern demonstrates that encapsulating the alloyed QDs with silica did not induce a phase change. The three diffraction peaks were more refined for the SiO₂-coated CdZnSeS QDs than for the TGA-CdZnSeS QDs, which we attribute to the surface modification of the alloyed nanocrystal.

3.2. Photophysical properties

Figures 4A and B show the absorption and PL emission spectra of luminescent TGA-capped and SiO₂-coated CdZnSeS QDs. Both alloyed nanocrystals displayed a band edge in the PL emission spectra with no evidence of deep-trap emission. A well-pronounced excitonic peak was evident in the absorption spectrum of the TGA-CdZnSeS QDs at 598 nm but was broadened slightly for the SiO₂-coated CdZnSeS QDs and red-shifted to 606 nm. The broadening and red shift of the excitonic peak of the SiO₂-coated CdZnSeS QDs are direct evidence of the surface modification process.

The PL emission wavelength of the TGA-CdZnSeS QDs was 624 nm, whereas that of the SiO₂-coated CdZnSeS QDs was 630 nm. The red shift of the PL emission also confirms the surface modification process. The full widths at half maximum (FWHM) of the alloyed nanocrystals were 36 nm for TGA-CdZnSeS QDs and 38 nm for SiO₂-coated CdZnSeS QDs. The FWHMs of the nanocrystals demonstrate that they exhibit a narrow emission line width, which is a unique advantage over traditional organic fluorophore dyes.

To assess the quality and to more effectively demonstrate the effect of the silanization process, we determined the PL QY of the alloyed nanocrystals. The PL QY of TGA-CdZnSeS QDs was 92%, whereas that of SiO₂-coated CdZnSeS QDs was 98%. In general, both alloyed nanocrystals exhibited remarkable PL QY, which directly confirm the improvement in the photophysical properties of the SiO₂-coated CdZnSeS QDs. The improvement in the PL QY of the QDs after silanization suggests that the fluorescence of the QDs was preserved. The mechanism of the silanization process involves the slow hydrolysis of 3-APTMS which resulted in a well-passivated arrangement on the QDs surface to form a thin layer of silica shell that de-shielded the fluorescence of the QDs from fluorescence loss. We therefore confirm that the silanization reaction employed in this work is viable and effective for producing silica-coated alloyed nanocrystals with remarkable optical properties for ultrasensitive biodetection.

The mechanism of the silanization reaction involves changing the surface state of the alloyed QDs with respect to the modification of the TGA thiol capping. The partial hydrolysis of 3-APTMS molecules in solution yielded a well-ordered array of silica coating onto the QD surface.

To further confirm the change in the surface state of the alloyed QDs, PL lifetime measurements were performed. Figures 4C and D present the PL decay curves of TGA-capped and SiO₂-coated CdZnSeS QDs. From the analysis of the decay curves, we observed a more well-ordered arrangement in the decay profile for SiO₂-coated CdZnSeS QDs than for TGA-CdZnSeS QDs. This difference in the decay profile confirms the surface modification of the QDs. The PL lifetime was fitted monoexponentially to a slow decay value of ~12.3 ns for the TGA-CdZnSeS QDs whereas for the SiO₂-coated CdZnSeS QDs a fast decay value of 2.8 ns and a slow decay value of 7.7 ns was obtained. These results indicate that the SiO₂-coated CdZnSeS QDs decayed faster than the TGA-CdZnSeS QDs. Because the PL lifetime depends on the nature of the surface-attached ligand, the fast decay exhibited by the SiO₂-coated CdZnSeS QDs directly confirms the surface state of the QDs that were modified during the silanization process and affirms the perfectly suppressed non-radiative recombination exciton states.

3.3. Biosensing of NV RNA

3.3.1. Conjugate formation

The covalent amide bond between the alloyed QD fluorophore reporter and MB was confirmed using FT-IR. Figure 5 shows the FT-IR spectra of the unconjugated alloyed SiO₂-coated CdZnSeS QDs and the SiO₂-coated CdZnSeS QD-MB bioprobe. In the spectrum of the unconjugated alloyed QDs, the band at 1541 cm⁻¹ was assigned to the asymmetric carboxylate

(-COO) group. For the QD-MB probe, the amide linkage was confirmed by the band at 1651 cm^{-1} for the primary amide bond and 1574 cm^{-1} for the secondary amide bond.

3.3.2. Detection of NV using SiO₂-CdZnSeS-MB

Having obtained a remarkable PL QY of 98% for the alloyed SiO₂-coated CdZnSeS QDs, an unprecedented PL signal reporting capability for NV RNA was anticipated. We therefore evaluated the ability of the SiO₂-CdZnSeS-MB bioprobe system to detect extremely low concentrations of NV genogroup II RNA. Figure 6A shows the PL signal spectra for the detection of NV RNA in a buffer solution using the SiO₂-CdZnSeS-MB probe. A steady increase in the PL intensity was achieved in the range of 2–16 copies/mL of NV RNA. A key feature of the detection system is the lack of a peak shift in the PL signal spectra. The lack of a peak shift demonstrates the high photostability of the modified alloyed QDs. The corresponding PL signal calibration curve is shown in Fig. 6B. The limit of detection (LOD) was calculated by multiplying the standard deviation (δ) of 10 separate measurements ($n = 10$) by 3 and dividing by the slope (K) of the linear calibration curve ($\text{LOD} = 3\delta/K$). The resulting LOD was 9.3 copies/mL.

3.3.3. Comparison to TGA-CdZnSeS-MB

To effectively demonstrate the advantages of the SiO₂-CdZnSeS-MB probe for NV RNA detection, we additionally investigated the efficacy of the TGA-CdZnSeS-MB probe for detecting extremely low concentrations of NV RNA under the same experimental conditions. We successfully detected NV RNA at 0–10 copies/mL using the TGA-CdZnSeS-MB probe, as shown in Fig. 6C (the corresponding PL signal calibration curve is shown in Fig. 6D). The LOD was 28.7 copies/mL, which is 3 times less sensitive than that of the SiO₂-CdZnSeS-MB

probe. This result confirms that the silica-encapsulated alloyed QDs produced an outstanding detection limit for NV RNA.

We believe two possible scenarios are responsible for the improved LOD of SiO₂-CdZnSeS QDs as a fluorophore reporter for NV RNA detection when compared to TGA-CdZnSeS QDs. The first is due to the improved PL QY of the QDs. A general concept in luminescence technology takes into consideration that the higher the PL QY of a fluorophore, the higher is its sensitivity for direct application (**Lima et al., 2013**). Surface dangling bonds on the QDs surface creates defect states that lowers the PL QY yield of the QDs. This imply that the higher the PL QY of the QD fluorophore, the lower is its defect states and a QD with PL QY of perfect unity (100%) transcends to a surface free from defect states (**Han et al., 2010; Peng et al. 1997**). We can tentatively infer that based on the higher PL QY of the SiO₂-CdZnSeS QDs, its surface is more sensitive to fluorescence signal generation for NV RNA than the fluorescence reporting signal of TGA-CdZnSeS QDs. The second possibility is that the distance between the FQ and SiO₂-CdZnSeS QD fluorophore reporter after hybridization of the MB with the target NV RNA is longer than the distance between TGA-CdZnSeS QDs and the FQ. This can be explained in terms of the surface capping on the QDs surface. TGA is a small thiol compound that induces the QDs to exhibit a shorter distance from the FQ after hybridization relative to the silica coating of the QDs which have extended functional groups that further stretches the distance of the QDs from the FQ after hybridization (Scheme. 1). Hence, the fluorescence of SiO₂-CdZnSeS-MB is more sensitive for NV RNA detection than TGA-CdZnSeS QDs.

3.3.4. Detection in human serum

To demonstrate the versatility of our detection system, NV RNA was detected in a complex biological medium, human serum. Figure 7A shows the PL signal emission spectra for the

detection of 0–12 copies/mL of NV RNA. A steady enhancement of the PL emission was obtained as the concentration of NV RNA increased. The corresponding PL calibration signal curve is shown in Fig. 7B. The LOD was 8.2 copies/mL, which is slightly lower than the value obtained in buffer medium. This result demonstrates that our detection system is ultrasensitive and versatile. Table 1 shows the comparison of the LOD of our detection system with reported values for the detection of NV genogroup II. Additionally, in comparison to the sensitivity of RT-PCR (the gold standard for nucleic acid detection) for NV detection, a commercial RIDAGENE NV RT-PCR detection kit has a LOD of 50 copies per reaction (**Dunbar et al., 2014**) while Dreier et al reported a LOD of 711 copies/mL for NV detection using RT-PCR (**Dreier et al., 2006**). The LOD comparison demonstrates that our detection system is more sensitive than traditional molecular test probes and RT-PCR.

3.3.5. Specificity

The specificity of the SiO₂-CdZnSeS-MB probe system for the detection of the target NV RNA was investigated by comparing the PL signal intensity generated for the detection of 16 copies/mL of the target NV RNA with the PL signal intensity obtained for the detection of a non-complementary dengue 1 virus RNA and influenza virus RNA. The concentration of non-complementary dengue 1 virus RNA and influenza virus RNA was fixed at 16 copies/mL. As shown in Fig. 7C, the PL signal intensity generated for the target NV RNA was strongly enhanced relative to the PL intensity of the probe without the target. By contrast, the PL signal intensities for the non-complementary dengue 1 virus RNA and influenza virus RNA of NV RNA were relatively quenched. These results provide direct evidence that our detection system is highly specific for the detection of the target NV RNA.

4. Conclusion

A new nanobiosensor for NV genogroup II RNA was developed using a modified SiO₂-coated CdZnSeS-MB bioprobe detection system. The photophysical properties of the alloyed QDs were improved by modifying the thiol-capped surface with a silica layer with a thickness of ~0.4 nm. Remarkably, the silanization process improved the PL QY value from 92% to 98%. We evaluated the abilities of the alloyed thiol-capped CdZnSeS-MB system and the SiO₂-coated CdZnSeS-MB system to detect extremely low concentrations of NV RNA. The SiO₂-CdZnSeS-MB probe was 3 times more sensitive than the thiol-capped CdZnSeS-MB. Our detection system is ultrasensitive, rapid, versatile (with the ability to detect NV RNA in human serum) and specific. Additionally, our detection system is more sensitive than traditional molecular test probes and could serve as an alternative for point-of-care diagnosis and rapid diagnosis of immunocompromised patients.

Acknowledgements

A Japan Society for the Promotion of Science (JSPS) postdoctoral fellowship for overseas researchers (P13454) is gratefully acknowledged. This work was supported by a Grant-in-Aid for JSPS fellow (No. 26-04354) and in part by the Grant-in-Aid for Scientific Research (S) under Grant 25220905 through the Ministry of Education, Culture, Sports, Science and Technology.

References

- Adegoke, O., Nyokong, T., Forbes, P.B.C., 2015. *J. Alloy. Compd.* 645, 443–449.
- Adegoke, O., Seo, M-W., Kato, T., Kawahito, S. Park, E.Y., 2016. *J. Mater. Chem. B* 4, 1489-1498.
- Anderson, R.E., Chan, W.C.W., 2008. *ACS Nano* 2, 1341-1352.

Ando, T., Monroe, S.S., Gentsch, J.R., Jin, Q., Lewis, D.C., Glass, R.I., 1995. *J. Clin. Microbiol.* 33, 64–71.

Barreiro, L.B., Henriques, R., Mhlanga, M.M., 2009. *Methods Mol. Biol.* 578, 255–276.

Bruchez, M., Moronne, M., Gin, P., Weiss, S., Alivisatos, A.P., 1998. *Science* 281, 2013–2016.

Caruge, J.M., Halpert, J.E., Wood, V., Bulovic, V., Bawendi, M.G., 2008. *Nat. Photonics* 2, 247–250.

Chan, W.C.W., Nie, S.M., 1998. *Science*, 281, 2016–2018.

Cloqston, J.D., Patro, A.K., 2011. *Methods Mol. Biol.* 697, 63–70.

Dunbar, N.L., Bruggink, L.D., Marshall, J.A., 2014. *Diagn. Micr. Infec. Dis.* 79, 317–321.

Han, H., Di Francesco, G., Maye, M.M., 2010. *J. Phys. Chem.* 114, 19270–19277.

Hodgson, D.R., Foy, C.A., Partridge, M., Pateromichelakis, S., Gibson, N.J., 2002. *Mol. Med.* 8, 227–237.

Kostrikis, L.G., Tyagi, S., Mhlanga, M.M., Ho, D.D., Kramer, F.R., 1998. *Science* 279, 1228–1229.

Li, J.J., Geyer, R., Tan, W., 2000. *Nucleic acids res.* 28, article e52.

Lima, N.B.D., Gonçalves, S.M.C., Júnior, S.A., Simas, A.M., 2013. *Sci. Reports* 3, 1–8.

Ma, W., Luther, J.M., Zheng, H., Wu, Y., Alivisatos, A.P., 2009. *Nano Lett.* 9, 2072–2077.

Medley, C.D., Drake, T.J., Tomasini, J.M., Rogers, R.J., Tan, W., 2005. *Anal. Chem.* 77, 4713–4718.

Patterson, S.S., Smith, M.W., Casper, E.T., Huffman, D., Stark, L., Fries, D., Paul, J.H., 2006. *J. Appl. Microbiol.* 101, 956–963.

Peng, X., Schlamp, M.C., Kadavanich, A.V., Alivisatos, 1997. A.P., *J. Am. Chem. Soc.* 119, 7019–7029.

Robilotti, E., Deresinski, S., Pinsky, B.A., 2015. *Clin. Microbiol. Rev.* 28, 134–164.

Rooney, B-L., Pettipas, J., Grudeski, E., Mykytczuk, O., Pang, X., Booth, T.F., Hatchette, T.F., LeBlanc, J.J., 2014. *Virology* 11, 1-7.

Santangelo, P., Nitin, N., LaConte, L., Woolums, A., Bao, G., 2006. *J. Virol.* 80, 682–688.

Seo, M.-W., Kagawa, K., Yasutomi, K., Takasawa, T., Kawata, Y., Teranishi, N., Li, Z., Halin, I.A., Kawahito, S., 2015. *IEEE Int. Solid-State Circuits Conf. (ISSCC) Dig. Tech. Papers* 198-199.

Swafford, L.A., Weigand, L.A., Bowers II, M.J., McBride, J.R., Rapaport, J.L., Watt, T.L., Dixit, S.K., Feldman, L.C., Rosenthal, S.J., 2006. *J. Am. Chem. Soc.* 128, 12299-12306.

Ünlü, C., Tosun, G.Ü., Sevim, S., Özçelik, S., 2013. *J. Mater. Chem. C* 1, 3026-3034.

Wang, X., Ren, X., Kahen, K., Hahn, M.A., Rajeswaran, M., Maccagnano-Zacher, S., Silcox, J., Cragg, G.E., Efros, A.L., Krauss, T D., 2009. *Nature* 459, 686–689.

Wu, C-S., Oo, M.K.K., Cupps, J.M., Fan, X., 2011. *Biosens. Bioelectron.* 26, 3870–3875.

Figure legends

Scheme 1. Schematic representation of the ligand-exchange reaction, silica encapsulation and conjugation and detection of NV RNA. The TGA thiol ligand was capped on the surface of the QDs via a ligand-exchange reaction. The QDs were first silanized with an amino group and then further silanized with a carboxylate group. The carboxylate-silanized QDs were conjugated to MB probes via EDC/NHS chemistry. The detection of viral NV RNA was accomplished via hybridization.

Fig. 1. TEM images of alloyed TGA-CdZnSeS QDs (A–C) and SiO₂-CdZnSeS QDs (D–F) at different magnifications.

Fig. 2. DLS spectra of TGA-CdZnSeS QDs (A) and SiO₂-CdZnSeS QDs (B). Zeta potential spectra of TGA-CdZnSeS QDs (C) and SiO₂-CdZnSeS QDs (D).

Fig. 3. Powder XRD spectra of TGA-CdZnSeS QDs and SiO₂-CdZnSeS QDs.

Fig. 4. UV/vis absorption and PL emission spectra of TGA-CdZnSeS QDs (A) and SiO₂-CdZnSeS QDs (B). PL lifetime decay curves of TGA-CdZnSeS QDs (C) and SiO₂-CdZnSeS QDs (D).

Fig. 5. FT-IR spectra of the unconjugated SiO₂-CdZnSeS QDs and the SiO₂-CdZnSeS QD-MB bioprobe.

Fig. 6. (A) PL-enhancement detection of NV RNA in buffer solution using the SiO₂-CdZnSeS QD-MB bioprobe and (B) the corresponding PL calibration curve. (C) PL enhancement detection of NV RNA in buffer solution using the TGA-CdZnSeS QD-MB bioprobe and (D) the corresponding PL calibration curve. The errors bars represent the standard deviation of three replicate measurements.

Fig. 7. (A) PL-enhancement detection of NV RNA in human serum using the SiO₂-CdZnSeS QD-MB bioprobe and (B) the corresponding PL calibration curve. (C) Specificity for the detection of NV RNA using the SiO₂-CdZnSeS QD-MB bioprobe and employing dengue 1 virus RNA and influenza virus RNA as negative controls. The errors bars represent the standard deviation of three replicate measurements.

Table 1. Comparison of the LOD of SiO₂-CdZnSeS-MB bioprobe with reported values for the detection of NV genogroup II.

Probe name	Technique	LOD (copies/mL)	Ref.
SiO ₂ -CdZnSeS QD-MB (BHQ-1)	Fluorescence enhancement	8.2	This work
EP-JV RT-PCR	Molecular test	3,981	Ronner et al. (2014)
EP-SR RT-PCR	Molecular test	31,623	Ronner et al. (2014)
NASBA MB assay	Molecular test	100	Patterson et al. (2006)

NASBA = Nucleic acid sequence-based amplification.

